Phenomenological Model for Projectile-Breakup Reactions

Constance Kalbach Walker
Triangle Universities Nuclear Laboratory, Duke University, Durham NC 27701, USA
(Dated: 1 December 2008)

A phenomenological model for light-projectile breakup is being developed using data for deuteron, ^{3}He, and α-particle induced reactions. Global systematics for the centroid energies, peak widths, angular distributions, and the target-mass-number dependence of the absolute breakup cross section have been developed. The incident-energy dependence of the cross section for each breakup channel still needs to be determined, and then the model will be included in preequilibrium reaction codes. This will permit the final benchmarking of these codes for complex-particle-induced reactions, in particular with regard to the initial particle-hole configuration used in the exciton preequilibrium model.

I. INTRODUCTION

One of the important goals of the FENDL-3 development project is the inclusion of deuteron-induced reactions in the data library. This will rely heavily on reaction model calculations, but general reaction model codes typically lack a model for the deuteron-breakup mechanism, which makes important contributions at almost all incident energies. The development of a robust projectile-breakup model is, therefore, an important priority for the FENDL-3 Coordinated Research Project.

Projectile breakup is here defined as the emission of a projectile fragment with a fairly narrow energy distribution peaked at an emission energy corresponding to the projectile velocity. The fragment is emitted with an angular distribution that is sharply peaked at forward angles—much more so than the surrounding and underlying cross section. When the undetected fragment interacts with the target nucleus, it forms a composite system that will then undergo energy equilibration. Particle emission occuring during and after that equilibration will need to be included in reaction model codes.

The question of projectile breakup, however, extends beyond deuterons. The breakup mechanism also makes significant contributions for reactions induced by ^{3}He ions and, at sufficiently high incident energies, by α-particles. Until a model for this mechanism is included in preequilibrium-model reaction codes, it is impossible to finalize the benchmarking of these codes for complex-particle-induced reactions. In particular, a definitive assignment of the initial particle-hole configuration in the exciton model cannot be made for complex-particle projectiles, because projectile breakup is expected to significantly reduce the amount of the total reaction cross section going into the main exciton-model equilibration calculations.

Given the importance of the projectile-breakup mechanism, both from a basic physics perspective and for energy applications, a phenomenological breakup model is being developed. It is designed for inclusion in the next release of the TUNL preequilibrium reaction code PRECO and in larger, more comprehensive Hauser-Feshbach model codes such as GNASH and TALYS.

II. DATABASE

The model that is being developed is based on data for deuteron, ^{3}He, and α-particle breakup. This yields a more robust and global model than one developed for deuteron breakup alone, because it uncovers the dependence of the breakup reaction on the energy required to separate the projectile into its constituent fragments. Continuum energy spectra measured at a variety of forward angles in a given reaction have been collected from the literature. All of the detected fragments are charged particles, so it will be assumed that neutron fragments follow generally the same systematics as proton fragments, except, of course, that there will be no Coulomb barrier in the exit channel. The data used are summarized in Table I. Other data at lower incident energies are available for ^{3}He and α-particle projectiles, but the breakup peaks, when present, are not distinct enough to be used in this study.

In order to develop a model for projectile breakup, the breakup peak must be differentiated from the remaining continuum cross section. This involves drawing a "background" underneath the obvious breakup peak, where the background is typically the usual preequilibrium cross section. This separation process was carried out for all of the spectra analyzed and is the greatest source of uncertainty in the present work. Even the assignment of uncertainties to the quantities extracted from the breakup peaks is a subjective process. Fortunately both the peak energies and their widths appear to be generally independent of the emission angle, so data from more than one angle can sometimes be used, reducing uncertainties. All analyses are carried out in the laboratory system.

TABLE I: Literature data used in developing the projectile breakup model.

Projectile	$E_{\rm inc}$ (MeV)	Targets	Ejectile	Angles	Ref.
d	14.8	Al, Cu , Zr, Cd, Pt	p	12°-85°	[1]
	14.8	11 others	p	30°	[1]
	15.0	^{62}Ni, Ta	p	23°-120°	[2]
	25.5	Al, ^{62}Ni, Nb, ^{119}Sn, Ta	p	20°-120°	[3]
	27.5	^{57}Fe, ^{116}Sn	p	20°-90°	[4]
	56	Al, ^{58}Ni, ^{90}Zr, ^{118}Sn, ^{209}Bi	p	9.5°-30°	[5]
	56	9 others	p	9.5°	[5]
	70	^{90}Zr, ^{208}Pb, ^{232}Th	p	20°-90°	[6]
	80	Al, ^{58}Ni	p	20°-90°	[6]
^{3}He	70, 90, 110	^{90}Zr	d	13°-30°	[7]
	70	6 others	d	13°	[7]
	90	11 others	d	13°	[7]
	70, 90	^{90}Zr	p	13°-40°	[7]
	130	Al, Co, Nb, Al	d	7.5°-21°	[8]
α	80	Al, ^{58}Ni, ^{90}Zr	p, d	6°-26°	[9]
	80	Al	t, ^{3}He	6°-26°	[9]
	140	Bi	^{3}He	13°-20°	[10]
	160	Al, ^{58}Ni, ^{90}Zr, Bi	p, d, t, ^{3}He	6°-26°	[9]

III. CENTROID ENERGIES

The simplest estimate of the energy of the breakup peak is that it corresponds to a fragment moving at the projectile velocity, so that

$$E_0 = E_{\rm inc}\, A_b/A_a, \tag{1}$$

where A_a and A_b are the mass numbers of the projectile and the detected fragment, respectively, and where $E_{\rm inc}$ is the projectile energy. The actual peak energy can be shifted slightly from this value by Coulomb deceleration in the entrance channel and by Coulomb acceleration in the exit channel. In the case of dissociative breakup, where both projectile fragments continue forward, the requirement of supplying the projectile's dissociation energy would lower the peak energy, but experimental peak energies for both ^{3}He and α-particle breakup exclude this as being a dominant mechanism. Instead, they point to "absorptive" breakup, in which the non-observed fragment interacts strongly with the target and the observed fragment is largely a spectator. For incident α particles, this observation is confirmed by coincidence measurements [11]. Thus the final expression for the peak energies is

$$E_0 = A_b/A_a\,(E_{\rm inc} - C_{\rm a}) + C_{\rm b}, \tag{2}$$

where $C_{\rm a}$ and $C_{\rm b}$ are the Coulomb barriers in the entrance and exit channels, respectively. The barrier $C_{\rm a}$ expressed in MeV is given by

$$C_{\rm a} = 1.44 Z_{\rm a}/D_0, \tag{3}$$

where $Z_{\rm a}$ is the atomic number of the projectile. A similar expression applies for $C_{\rm b}$. Here D_0 is the effective target-projectile separation at the point of interaction and is given in femtometers.

Using the experimental peak positions for the heaviest targets (the ones with the largest Coulomb barriers), estimates of the Coulomb shifts in the peak positions have been used to extract estimates for D_0. These results have been fit with the formula

$$D_0 = r_0 A^{1/3} + 1.2, \tag{4}$$

where r_0 is an effective radius parameter that depends only on the incident energy and is found to have the form

$$r_0 = 1.2 + \frac{5}{1+\exp(E_{\rm inc}/30)}\,. \tag{5}$$

Here A is the target mass number, and both D_0 and r_0 are given in femtometers. The projectile energy $E_{\rm inc}$ is assumed to be given in MeV. Figure 1 shows the experimentally-derived and fitted values for $r_0 = (D_o - 1.2)/A^{1/3}$ as a function of the incident energy for all breakup channels investigated. It is assumed that this formula will apply to lighter targets as well, since the data uncertainties do not allow the Z-dependence of r_0 to be probed.

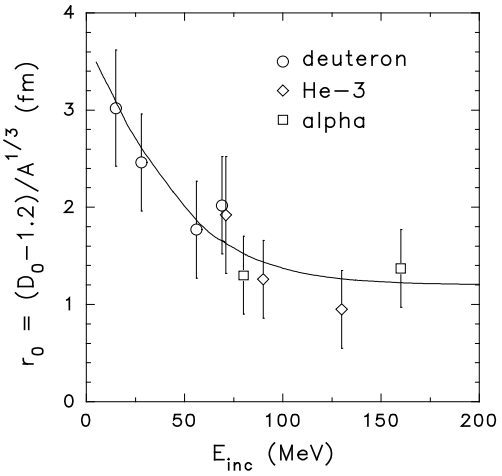

FIG. 1: Effective radius parameter for projectile breakup. The points show the values inferred from the Coulomb shifts in the energies of the breakup peaks in literature data for the indicated projectiles. In each case the results from the heaviest available target were chosen, since these have the largest energy shifts. The solid curve shows the fitted dependence given by Eq. (5). Its asymptotic value is 1.2 fm.

The systematic peak energies for (d,p) breakup obtained from Eqs. (2)-(5) are shown in Fig. 2 along with the experimental values.

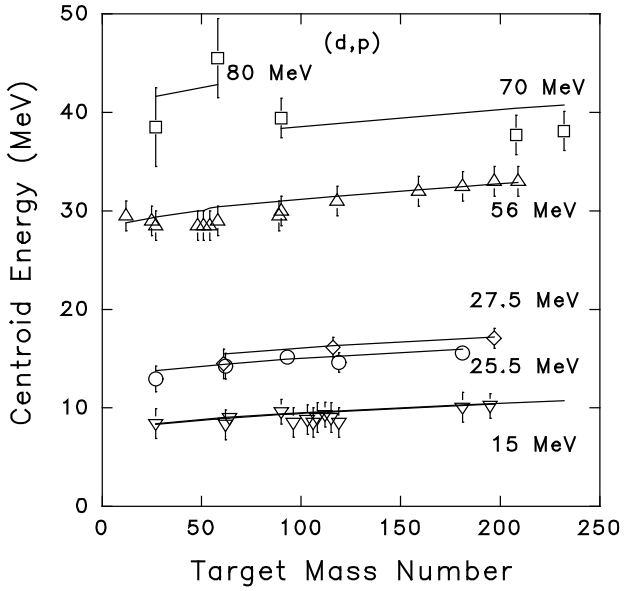

FIG. 2: Experimental peak energies for (d,p) breakup at the indicated incident energies. The points show the values extracted from the data, while the lines represent the systematic values obtained from Eq. (2)

IV. PEAK SHAPES AND WIDTHS

A. Basic systematics

The breakup peaks are assumed to have a Gaussian shape so that

$$\frac{d\sigma_{\rm bu}}{d\varepsilon} = \sigma_{\rm bu}\frac{1}{\sqrt{2\pi}w}\exp\left[-\frac{(\varepsilon - E_0)^2}{2w^2}\right], \tag{6}$$

where w is the peak width and ε is the energy of the observed breakup fragment.

The full width at half maximum (FWHM) of the breakup peaks is denoted as $F = 2.65w$. It appears to be largely independent of emission angle and only weakly dependent on target mass number. A workable empirical formula for this width, given in MeV, is

$$F = 62\left[1 - \frac{1}{\exp(E_{\rm inc}/173)}\right]\left[1 - \frac{A}{155(S_{\rm a,b})^2}\right] - 3\,\Theta(A_a - A_b - 1.5), \tag{7}$$

where $S_{\rm a,b}$ is the energy required to separate the projectile into the observed fragment b and its complement, and Θ is the Heaviside step function, which is zero for a negative argument and one for a positive argument. Both $E_{\rm inc}$ and $S_{\rm a,b}$ The last term in Eq. (7) lowers the FWHM for (^{3}He,p), (α,p) and (α,d) breakup relative to the channels where only a single nucleon is absorbed by the target. This difference between channels with $A_{\rm b} = A_{\rm a} - 1$ and those with $A_{\rm b} < A_{\rm a} - 1$ was unexpected but shows up again in the angular distribution systematics discussed below. A comparison of widths obtained from Eq. (7) with the experimental values for deuteron-induced reactions is shown in Fig. 3.

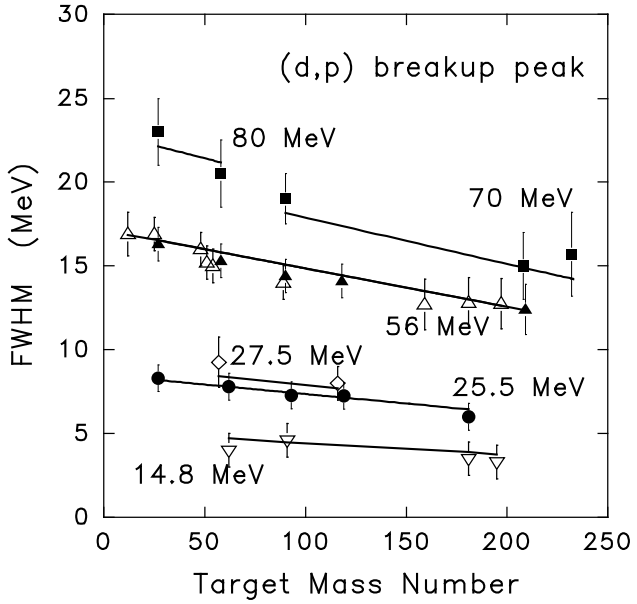

FIG. 3: FWHM for deuteron breakup peaks at the incident energies shown in the figure. The points show the experimental values extracted from data in the literature, while the lines are obtained from Eq. (7).

The peak shapes, widths, and, in extreme cases, even their positions can be modified by either the Coulomb barrier or the maximum-energy cutoff in the spectrum due to energy conservation. These effects have not been observed in deuteron breakup, but the maximum-energy-cutoff effect has been seen in (α,t) and (α,^{3}He) breakup. Both effects have been included in the model.

B. Modifications from the Maximum-Energy Cutoff and the Coulomb Barrier

Some of the (α,t) and (α,^{3}He) breakup peaks appear to be assymetric, with the higher emission energy side being narrower. This is due to restrictions placed on the peak width by the kinematic limit on the energy of the observed

fragment. This effect can be included in the model by leaving the peak in its normal position and using different widths for the two halves of the Gaussian distribution. If $\epsilon_{\rm max}$ is the maximum energy kinematically allowed and $H = F/2$ is the half width at half maximum from the base systematics, then the full width at half maximum becomes

$$F_{\rm eff} = H + \min\left[H, 0.6(\epsilon_{\rm max} - E_0)\right] \tag{8}$$

where the factor of 0.6 is an empirical estimate. There are additional modifications if $\epsilon_{\rm max} < E_0$, but this condition has not been observerd, and so this detail is omitted in the present report. In addition, it remains to be seen whether the peak narrowing produced by the maximum energy cutoff changes the size of the breakup cross section or simply redistributes it in energy.

If the Coulomb barrier is high enough relative to the energy of the breakup peak, then the peak shape should be multiplied by a barrier penetrability factor:

$$T = \left[1 + \exp\left(\frac{3(C_{\rm b} - \varepsilon)}{C_{\rm b}}\right)\right] \tag{9}$$

where ε is the energy of the observed fragment. Again, it is still unknown whether this reduces the breakup cross section or simply shifts it to higher emission energies.

V. BREAKUP ANGULAR DISTRIBUTIONS AND A-DEPENDENCE OF THE BREAKUP CROSS SECTION

A. Base Systematics

For a given breakup channel and incident energy, comparing the data from a variety of targets shows that at each emission angle the breakup cross section is approximately proportional to $(D_0)^2$. Thus the data from different targets can be divided by $(D_0)^2$ and plotted as a function of emission angle in the laboratory system in order to study the average angular distribution systematics.

With the exception of the (d,p) breakup peaks at an incident energy of around 15 MeV, the remaining data show an angular distribution that is a negative exponential in the emission angle θ. This is shown in Fig. 4.

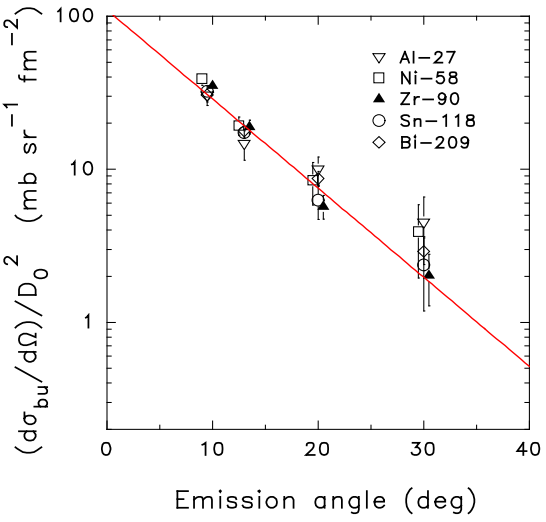

FIG. 4: Normalized angular distributions for (d,p) breakup at 56 MeV. The points show the experimental breakup cross sections divided by $(D_0)^2$ as a function of angle, while the line shows the best fit with an exponential in the emission angle.

The points in this and similar plots for different breakup channels and different incident energies were fit with a dependence of the form

$$\frac{d\sigma_{\rm bu}(\theta)}{d\Omega}\frac{1}{(D_0)^2} = Ke^{-a_{\rm bu}\theta}. \tag{10}$$

where K and $a_{\rm bu}$ were the fitting parameters. The results of this fitting are also shown in Fig. 4. The values of $a_{\rm bu}$ where then studied to look for systematics. Here again, as was the case for the peak widths, a difference seems to emerge between the breakup channels with $A_{\rm b} = A_{\rm a} - 1$ and those with $A_{\rm b} < A_{\rm a} - 1$. In the latter case, the angular distribution slope appears to be independent of incident and emission energy. On the other hand, for $A_{\rm b} = A_{\rm a} - 1$ (the case of interest for deuteron breakup), the results show a definite energy dependence and can be parameterized in terms of either the incident energy or the peak energy. The parameterization in terms of the peak energy, E_0, gives a slightly better fit and is more consistent with the systematics for the underlying continuum angular distributions, which are likewise expressed as a function of the emission energy. The empirical slope parameters $a_{\rm bu}$ are shown as a function of E_0 in Fig. 5. The fitted slope parameters given in rad^{-1} are

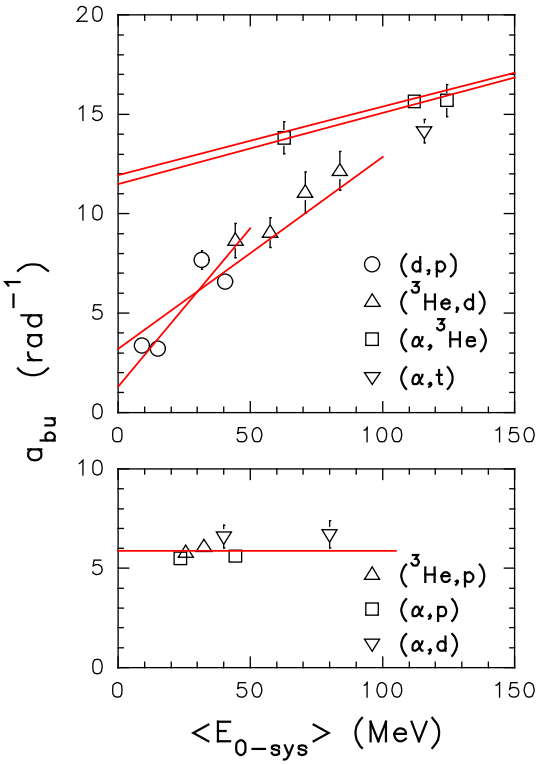

FIG. 5: Empirical values for the breakup-angular-distribution slope parameter $a_{\rm bu}$ as a function of the average centroid energy of the targets for which angular distributions were determined. The lines show the systematics given by Eq. (11)

$$a_{\rm bu} = \begin{cases} 0.58 S_{\rm ab} + 0.177 E_0 M_{\rm a}/S_{\rm ab} & \text{for } A_{\rm b} = A_{\rm a} - 1 \\ 5.87 & \text{for } A_{\rm b} < A_{\rm a} - 1 \end{cases} . \tag{11}$$

B. Coulomb Dip at Forward Angles

For (d,p) breakup at around 15 MeV, the data for the heavier targets show that the angular distributions are low at forward angles, gradually increase, and then at higher angles begin to follow the normal exponential falloff with θ. The width and depth of the dip at forward angles are correlated with the size of the Coulomb barrier relative to the incident energy. The dip has been parameterized as an angular penetrability factor multiplying the basic angular distribution of Eq. (10). The evidence here is clear that the forward-angle dip does not reduce the breakup cross section but simply redistributes it to larger angles. Thus, in the presence of such a dip, the angular distribution

becomes

$$\frac{d\sigma_{\rm bu}(\theta)}{d\Omega}\frac{1}{(D_0)^2} = \frac{K^{'}e^{-a_{\rm bu}\theta}}{1+\exp[(\theta_0-\theta)/d]}, \tag{12}$$

$$\theta_0 = 4.4\ \left(C_{\rm a}/E_{\rm inc}\right)^2, \tag{13}$$

$$d = \min(1.5/E_{\rm inc}, \theta_0/3). \tag{14}$$

Here θ_0 is the angular "barrier" and d is its width. Both are given in units of radians. The normalization factor $K^{'}$ is adjusted so as to preserve the normalization of the breakup cross section obtained for lighter targets. The details of its form, expressed in terms of K, θ_0, and d, are omitted here. The results obtained from Eqs. (12)-(14) are shown in Fig. 6 along with the corresponding data. If the same equations are applied for (d,p) breakup at 25.5 MeV, the

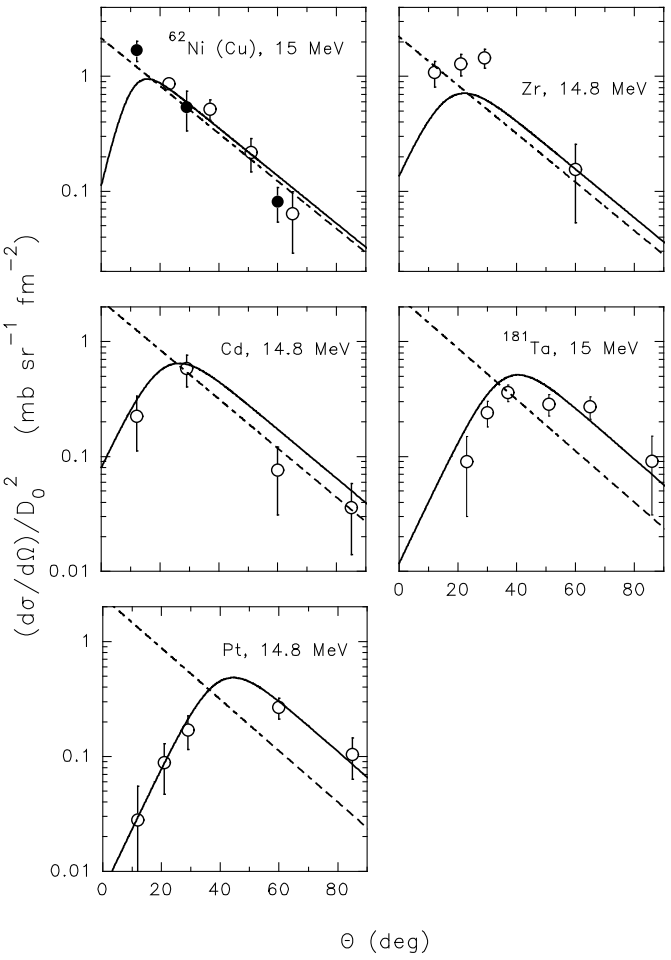

FIG. 6: Angular distributions for the (d,p) breakup peaks at incident energie of 14.8 and 15.0 MeV. The points show the results obtained from experimental spectra, the dashed curves show the results from Eq. (10), while the solid curves are obtained from Eq. (12)

resulting forward angle dip occurs at smaller angles than those for which data are available.

The results here for the Coulomb dip in the angular distributions must be regarded as very preliminary, since they have been derived and tested only for (d,p) breakup at around 15 MeV, though they are consistent with the data at 25.5 MeV. As the emission energy increases, θ_0 should get progressively smaller, and at incident energies above 25 MeV the Coulomb dip can probably be safely ignored, as was done in the main analysis.

VI. REMAINING WORK

Work is continuing on the absolute cross section for projectile breakup. It has already been mentioned that the cross section for a given breakup channel and incident energy is proportional to $(D_0)^2$, but the dependence on incident energy and on the specific breakup channel has yet to be determined.

Once a complete model for projectile breakup has been obtained, it will need to be programmed into a computer code and the results compared with the experimental breakup peaks. Following that, the program will be included in the TUNL preequilibrium reaction code PRECO [12], and the absorbed (or non-observed) fragment will be allowed to initiate an equilibration process as described by the exciton model. Once that coding has been completed, a larger body of full energy spectra will be analyzed in order to complete the determination of the initial particle-hole configuration in the exciton model for complex-particle-induced reactions.

---

[1] E. W. Hamburger, B. L. Cohen, and R. E. Price, Phys. Rev., **121** (1961) 1143.

[2] J. Kleinfeller, J. Bisplinghoff, J. Ernst, T Mayer-Kuckuk, G. Baur, B. Hoffmann, R. Shyam, F. Rősel, and D. Trautman, Nucl. Phys., **A370** (1981) 205.

[3] J. Pampus, J. Bisplinghoff, J. Ernst, T. Mayer-Kuckuk, J. Rama Rao, G. Baur, F. Rősel, and D. Trautman, Nucl. Phys., **A311** (1978) 141.

[4] A. Chavarier, N. Chevarier, A. Demeyer, A. Alevra, I. R. Lukas, M. T. Magda, and M. E. Nistor, Nucl. Phys., **A237** (1975) 354.

[5] N. Matsuoka, M. Kondo, A. Shimizu, T. Saito, and S. Nagamachi, Nucl. Phys., **A345** (1980) 1.

[6] J. R. Wu, C. C. Chang, and H. D. Holmgren, Phys. Rev. C, **19** (1979) 370.

[7] N. Matsuoka, A. Shimizu, K. Hosono, T. Saito, M. Kondo, H. Sakaguchi, Y. Toba, A. Goto, and F. Ohtani, Nucl. Phys., **A311** (1978) 173.

[8] A. Djaloeis, J. Bojowald, S. Gopal, W. Oelert, N. G. Puttaswamy, P. Turek, and C. Mayer-Bőricke, Phys. Rev. C, **27** (1983) 2389

[9] J. R. Wu, C. C. Chang, H. D. Holmgren, and R. W. Koontz, Phys. Rev. C, **20** (1979) 1284.

[10] J. R. Wu, C. C. Chang, and H. D. Holmgren, Phys. Rev. Lett., **40** (1978) 1013.

[11] R. W. Koontz, C. C. Chang, H. D. Holmgren, and J. R. Wu, Phys. Rev. Lett., **43** (1979) 1862.

[12] Constance Kalbach Walker, "Users Manual for PRECO-2006," unnumbered report, Triangle Universities Nuclear Laboratory, February 2007, available from the National Nuclear Data Center at Brookhaven National Laboratory, http://www.nndc.bnl.gov/nndcscr/model-codes/preco-2006/